Relativistic cluster calculation of ligand-field multiplet effects on cation L-2,L-3 x-ray-absorption edges of SrTiO3, NiO, and CaF2

AUTHOR(S):

Ogasawara, K; Iwata, T; Koyama, Y; Ishii, T; Tanaka, I; Adachi, H

CITATION:

Ogasawara, K ...[et al]. Relativistic cluster calculation of ligand-field multiplet effects on cation L-2,L-3 x-ray-absorption edges of SrTiO3, NiO, and CaF2. PHYSICAL REVIEW B 2001, 64(11): 115413.

ISSUE DATE:

2001-09-15

URL:

http://hdl.handle.net/2433/39849

PHYSICAL REVIEW B, VOLUME 64, 115413

Relativistic cluster calculation of ligand-field multiplet effects on cation $L_{2,3}$ x-ray-absorption edges of $SrTiO_3$, NiO, and CaF_2

Kazuyoshi Ogasawara, Takahiro Iwata, Yukinori Koyama, and Takugo Ishii
Department of Materials Science and Engineering, Kyoto University, Sakyo-ku, Kyoto 606-8501, Japan

Isao Tanaka
Department of Energy Science and Technology, Kyoto University, Sakyo-ku, Kyoto 606-8501, Japan

Hirohiko Adachi
Department of Materials Science and Engineering, Kyoto University, Sakyo-ku, Kyoto 606-8501, Japan
(Received 16 January 2001; published 27 August 2001)

A totally nonempirical relativistic cluster calculation of transition-metal $L_{2,3}$-edge x-ray-absorption near-edge structure including configuration interaction has been performed. A remarkable predictive power of this calculation has been demonstrated for three contrasting materials with different *d*-electron numbers and different coordination numbers ($SrTiO_3$, NiO, and CaF_2) by excellent reproduction of both the absolute peak energies and their relative intensities without any empirical parameters.

DOI: 10.1103/PhysRevB.64.115413 PACS number(s): 78.70.Dm, 71.15.Rf, 78.20.Bh

I. INTRODUCTION

Both x-ray-absorption near-edge structure (XANES) and electron-energy-loss near-edge structure (ELNES) have been recognized as valuable probes to investigate the structural environment and chemical states of particular atomic species in a given compound.[1] Sharp peaks at the thresholds of L_3-edge and L_2-edge XANES and ELNES of $3d$ transition metals are attributed to electric-dipole transitions from the $2p_{3/2}$ and $2p_{1/2}$ core states to the unoccupied $3d$ levels. Within the single-particle picture (one-electron approximation), the final states in both edges are equivalent and their intensity ratio (branching ratio) should follow the statistical value 2:1 expected from the ratio of the initial states. On the contrary, the observed branching ratio is generally far from this ideal value, mainly due to the correlations among the $2p$ core hole and the $3d$ electrons, which can be rephrased in the terminology of atomic physics as ''multiplet effects.''

Currently, the most prevalent theoretical analysis is the crystal-field multiplet calculation developed by de Groot *et al.*,[2] where crystal-field effects are incorporated into an atomic multiplet program using group theoretical formalism. In the actual computational procedure, crystal fields are included as empirical parameters and the Slater integrals are reduced to simulate hybridization of anion orbitals and electron correlations. A great number of transition-metal compounds have been investigated by this atomic multiplet approach, and the parameters have been determined for many ''fingerprint'' spectra.[3]

Although this empirical approach has greatly contributed to interpret the observed spectra and to clarify the underlying physics, the advanced scientific technology requires investigation of progressively complicated materials where there is no available fingerprint spectra to compare. The lower the symmetry, the more parameters are required to account for all possible interactions. The detailed analysis sometimes requires the consideration of the so-called ''ligand hole,'' [4] which further introduces a new set of parameters. Since increase of parameters generally obscures information on explicit local atomic arrangements, establishment of a nonempirical theoretical approach with reliable predictive power is indispensable for the analysis of a variety of advanced materials without ambiguity.

In the present paper we perform a totally nonempirical relativistic cluster calculation of $L_{2,3}$-edge XANES and ELNES including configuration interaction (CI) and demonstrate its excellent predictive power by choosing three simple but contrasting cases: Ti^{4+} in $SrTiO_3$ (d^0 with sixfold coordination), Ni^{2+} in NiO (d^8 with sixfold coordination), and Ca^{2+} in CaF_2 (d^0 with eightfold coordination). The same procedure is generally applicable to any d^N ions with any symmetry. Although these spectra had been already successfully interpreted based on the traditional empirical approach,[3] reproduction of the same results without any empirical parameters is a remarkable theoretical progress toward the prediction of fingerprint spectra for unknown materials. Moreover, the origins of the peaks are analyzed in more detail based on the nonempirical configuration analysis of the many-electron wave functions in the present work.

II. COMPUTATIONAL PROCEDURE

The adopted model clusters are $(TiO_6)^{8-}$, $(NiO_6)^{10-}$, and $(CaF_8)^{6-}$ with O_h (octahedral) symmetry, which were constructed according to the crystal structure of $SrTiO_3$, NiO, and CaF_2, respectively, where the slight distortion of NiO below the Néel point was neglected for simplicity. Several thousand point charges were located at the external atomic positions so as to reproduce the effective Madelung potential.

Since the CI calculation for all N electrons in the cluster is unrealistically demanding, we adopted a relativistic many-electron Hamiltonian for selected n electrons,

TABLE I. Occupancy of each type of orbital in the electronic configurations considered for the calculation of Ti^{4+} and Ca^{2+} $L_{2,3}$ edges. GS and ES denote the ground-state configuration and the excited-state configuration, respectively. The number of Slater determinants (SD's) in each configuration is listed in the sixth column. The labels in the last column are used in the configuration analysis (Fig. 2).

	$2p_{1/2}$	$2p_{3/2}$	t_{2g}	e_g	Number of SD's	Label
GS	2	4	0	0	1	A
ES	2	3	1	0	24	B
	2	3	0	1	16	C
	1	4	1	0	12	D
	1	4	0	1	8	E

$$H=\sum_{i=1}^{n} h(\mathbf{r}_i)+\sum_{i=1}^{n}\sum_{j>i}^{n}\frac{1}{|\mathbf{r}_i-\mathbf{r}_j|}, \tag{2.1}$$

where

$$h(\mathbf{r}_i)=c\,\boldsymbol{\alpha}\mathbf{p}_i+\beta c^2-\sum_{\nu}\frac{Z_\nu}{|\mathbf{r}_i-\mathbf{R}_\nu|}+V_0(\mathbf{r}_i). \tag{2.2}$$

Here $\boldsymbol{\alpha}$, β are the Dirac matrices, c is the velocity of light, $\mathbf{p}_i$ is the momentum operator, Z_ν is the charge of the νth nucleus, and $V_0(\mathbf{r})$ is the potential from the other $N-n$ electrons, and atomic units ($m=e=\hbar=1$) are used throughout this paper. The explicit form of $V_0(\mathbf{r})$ was derived by Watanabe and Kamimura[5] as

$$V_0(\mathbf{r})=\int\frac{\rho_0(\mathbf{r}')}{|\mathbf{r}-\mathbf{r}'|}d\mathbf{r}'+\frac{3}{4}\times\left[\frac{\rho(\mathbf{r})V_{\mathrm{xc}}\{\rho(\mathbf{r})\}-\rho_0(\mathbf{r})V_{\mathrm{xc}}\{\rho_0(\mathbf{r})\}}{\rho_1(\mathbf{r})}-V_{\mathrm{xc}}\{\rho_1(\mathbf{r})\}\right], \tag{2.3}$$

where ρ_1 is the charge density of the selected n electrons, ρ_0 is the charge density of the other $N-n$ electrons, ρ is the charge density of all N electrons ($\rho=\rho_0+\rho_1$), and V_{xc} is the Slater's exchange-correlation potential.[6] In this approach, the Coulomb interaction and the exchange-correlation interaction among the selected n electrons are considered explicitly by the second term of Eq. (2.1), while those interactions between the n electrons and the $N-n$ electrons are included in the form of $V_0(\mathbf{r})$.

As the basis functions to diagonalize the Hamiltonian (2.1), all the possible Slater determinants for the ground-state (GS) configuration and the excited-state (ES) configuration including a core hole were prepared. In the present work, the cation $2p$ orbitals and the molecular orbitals (MO's) mainly consisting of the cation $3d$ (t_{2g} and e_g) were considered. In the case of Ti^{4+} and Ca^{2+}, six electrons occupy these orbitals. Therefore, there is only one Slater determinant in the GS configuration, while there are 60 in the ES configuration as listed in Table I, where the Slater determinants are classified according to the occupancy for each type of orbitals. Similarly, in the case of Ni^{2+}, 14 electrons occupy these orbitals. Thus there are 45 and 60 Slater determinants in the GS and ES configurations respectively, as listed in Table II.

TABLE II. Occupancy of each type of orbital in the electronic configurations considered for the calculation of Ni^{2+} $L_{2,3}$ edge. GS and ES denote the ground-state configuration and the excited-state configuration, respectively. The number of Slater determinants (SD's) in each configuration is listed in the sixth column. The labels in the last column are used in the configuration analysis (Fig. 2).

	$2p_{1/2}$	$2p_{3/2}$	t_{2g}	e_g	Number of SD's	Label
GS	2	4	6	2	6	A
	2	4	5	3	24	B
	2	4	4	4	15	C
ES	2	3	6	3	16	D
	2	3	5	4	24	E
	1	4	6	3	8	F
	1	4	5	4	12	G

The relativistic four-component MO's to construct the above Slater determinants were calculated self-consistently based on the Dirac-Fock-Slater formalism using the relativistic SCAT computation code originally developed by Rosén *et al.*,[7] which has been recently utilized to clarify the relativistic effects in actinide compounds.[8] The numerically generated four-component relativistic atomic orbitals ($1s\sim4p$ for Ti, Ni, and Ca and $1s\sim2p$ for O and F) were used as the basis functions and all integrals were carried out numerically using 100 000 sampling points.

The matrix elements of H between two Slater determinants, Φ_p and Φ_q, can be generally expanded as

$$H_{pq}=\langle\Phi_p|H|\Phi_q\rangle=\sum_{i=1}^{L}\sum_{j=1}^{L}A_{ij}^{pq}\langle i|h|j\rangle+\sum_{i=1}^{L}\sum_{j=1}^{L}\sum_{k=1}^{L}\sum_{l=1}^{L}B_{ijkl}^{pq}\langle ij||kl\rangle, \tag{2.4}$$

where L is the number of the considered orbitals and

$$\langle i|h|j\rangle=\sum_{\lambda=1}^{4}\sum_{\mu=1}^{4}\int\phi_{i\lambda}^{*}(\mathbf{r})h_{\lambda\mu}(\mathbf{r})\phi_{j\mu}(\mathbf{r})d\mathbf{r} \tag{2.5}$$

$$\langle ij||kl\rangle=\sum_{\lambda=1}^{4}\sum_{\mu=1}^{4}\int\int\phi_{i\lambda}^{*}(\mathbf{r}_1)\phi_{j\mu}^{*}(\mathbf{r}_2)\times\frac{1}{|\mathbf{r}_1-\mathbf{r}_2|}\phi_{k\lambda}(\mathbf{r}_1)\phi_{l\mu}(\mathbf{r}_2)d\mathbf{r}_1d\mathbf{r}_2. \tag{2.6}$$

Here $\phi_{i\lambda}$ ($\lambda=1,2,3,4$) is the λth component of the ith relativistic MO and $h_{\lambda\mu}(\mathbf{r})$ is the $\lambda\mu$ element of $h(\mathbf{r})$. The coefficients A_{ij}^{pq} and B_{ijkl}^{pq} can be easily obtained by expanding the Slater determinants.

By diagonalizing the Hamiltonian matrix (2.4), we can obtain the many-electron energy levels and the corresponding eigenvectors. Using the eigenvectors, the many-electron

wave functions are generally expressed as a linear combination of the Slater determinants,

$$\Psi_i = \sum_{p=1}^{M} C_{ip}\Phi_p , \tag{2.7}$$

where M is the number of the Slater determinants. Since all integrals are performed numerically without requiring any particular symmetry properties of the system, this approach can be applied to systems with any symmetry. In fact, we have recently calculated the d-d transitions of Cr^{3+} in ruby based on a similar approach within the nonrelativistic framework, and the spectrum caused by the slight trigonal distortion of the system was successfully reproduced.[9]

In principle, both the energy levels in the GS configuration and those in the ES configuration should be obtained directly by a simple diagonalization of H. However, we have found that this direct diagonalization slightly overestimates (typically by less than 1%) the energy difference between the GS and ES configurations. This overestimation is probably due to the underestimation of the correlation effects between the selected n electrons and the other $N-n$ electrons in the ES configuration, because the form of $V_0(\mathbf{r})$ describing these interactions was basically derived from the ground-state electronic structure. Mathematically, these correlation effects can be included explicitly by increasing n (number of the explicitly treated electrons) and L (number of the considered orbitals). However, the accompanying drastic increase of Slater determinants would be computationally unfavorable.

On the other hand, in the single-particle picture, these correlation effects can be included as the electronic (orbital) relaxation during transition using the so-called Slater's transition-state (TS) method.[6] As a result, the total-energy difference between two configurations in a many-electron system can be well approximated by the orbital-energy difference between the relevant single-electron orbitals in the Slater's transition-state calculation, as demonstrated by the successful reproduction of variety of XANES and ELNES for some oxides and nitrides.[10–12] Therefore, we adopted a combination of the CI calculation and the TS calculation in the present paper. In this approach, the energy separation between the GS and ES configurations was determined by a single-particle TS calculation.

Considering the negligibly small interaction between the GS and ES configurations, the above condition can be accomplished by modifying the matrix elements of H as

$$H'_{pq} = \begin{cases} H_{pq} & (\mathrm{GS}), \\ H_{pq} + \delta_{pq}\Delta E & (\mathrm{ES}), \end{cases} \tag{2.8}$$

where ΔE is the energy shift due to the electronic relaxation during transition, which can be expressed as $\Delta E = E_{\mathrm{TS}} - E_{\mathrm{CI}}$ using the transition energy estimated by the TS calculation (E_{TS}) and that estimated by the simple CI calculation (E_{CI}). In the present work, ΔE was calculated using the initial-state configuration and the lowest-excited-state configuration. For example, in the case of Ti^{4+}, ΔE was estimated using configurations A and B in Table I. Thus E_{CI} was calculated as the difference between the energy of configuration A and the average energy of configuration B, while E_{TS} was calculated as the orbital-energy difference between $2p_{3/2}$ and t_{2g} in the $(2p_{1/2})^2(2p_{3/2})^{3.5}(t_{2g})^{0.5}(e_g)^0$ configuration. Similarly, configurations A and D in Table II were used for the calculation of Ni^{2+}, while configurations A and C in Table I were used for Ca^{2+}.

The oscillator strength of the electric-dipole transition averaged over all polarizations is generally expressed as

$$I_{if} = \frac{2}{3}(E_f - E_i)\left|\left\langle \Psi_i \left| \sum_{j=1}^{n} \mathbf{r}_j \right| \Psi_f \right\rangle\right|^2 , \tag{2.9}$$

where Ψ_i and Ψ_f are the many-electron wave functions for the initial and final states, with energies E_i and E_f. Using Eq. (2.7), the integral in Eq. (2.9) can be expanded as

$$\begin{aligned} \left\langle \Psi_i \left| \sum_{j=1}^{n} \mathbf{r}_j \right| \Psi_f \right\rangle &= \sum_{p=1}^{M}\sum_{q=1}^{M} C_{ip}^{*} C_{fq} \left\langle \Phi_p \left| \sum_{j=1}^{n} \mathbf{r}_j \right| \Phi_q \right\rangle \\ &= \sum_{p=1}^{M}\sum_{q=1}^{M} C_{ip}^{*} C_{fq} \sum_{k=1}^{L}\sum_{l=1}^{L} A_{kl}^{pq} \langle k|\mathbf{r}|l\rangle , \end{aligned} \tag{2.10}$$

where

$$\langle k|\mathbf{r}|l\rangle = \sum_{\lambda=1}^{4} \int \phi_{k\lambda}^{*}(\mathbf{r})\mathbf{r}\phi_{l\lambda}(\mathbf{r})d\mathbf{r}. \tag{2.11}$$

In the actual calculation of Eqs. (2.5), (2.6), and (2.11), the summation was taken over the major components ($\lambda = 1,2$ and $\mu = 1,2$) and the terms relevant to the minor components ($\lambda = 3,4$ or $\mu = 3,4$) were neglected, because their compositions in a molecular orbital are less than 0.1% in the present case.

III. RESULTS AND DISCUSSIONS

In order to illuminate the ligand-field multiplet effects, theoretical spectra based on the one-electron approximation [single-particle (SP) calculation] were compared with the final theoretical spectra including the multiplet effects, as reported for Ti^{4+} based on the traditional atomic calculation.[13]

The SP calculations were carried out using the Slater's transition-state method, where a half electron was removed from $2p_{3/2}$ or $2p_{1/2}$ and put in the lowest unoccupied orbital for the L_3 and L_2 edges, respectively. In this case, the oscillator strengths were calculated by

$$I_{if} = \frac{2}{3}(\varepsilon_f - \varepsilon_i)|\langle \phi_i|\mathbf{r}|\phi_f\rangle|^2 , \tag{3.1}$$

where ϕ_i and ϕ_f are the single-electron orbitals for the initial and final states, with orbital energies ε_i and ε_f.

In Fig. 1, the calculated peak energies and the oscillator strengths are shown by solid straight lines and compared with the experimental spectra reported by several authors.[14,15,2] Here we do not intend to perform a complete simulation of the observed spectra, since the broadening factor of each peak is determined by variety of phenomena such

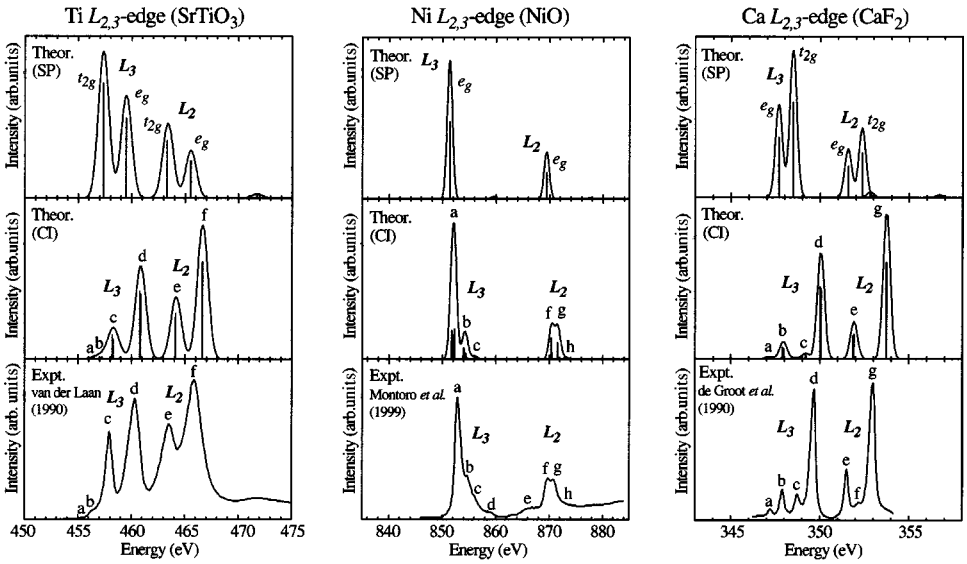

FIG. 1. Theoretical peak energies and peak intensities of the $L_{2,3}$-edge XANES for Ti^{4+} in $SrTiO_3$, Ni^{2+} in NiO, and Ca^{2+} in CaF_2 using $(TiO_6)^{8-}$, $(NiO_6)^{10-}$, and $(CaF_8)^{6-}$ clusters, respectively, obtained by the single-particle (SP) calculation (top), those obtained by the relativistic CI calculation (middle), and the corresponding experimental XANES spectra taken from Refs. 14, 15, and 2 (bottom). In the calculated results, the curves obtained by the simple Gaussian broadening are shown together for easy comparison with the experimental spectra.

as the core-hole lifetime broadening, the Coster-Kronig Auger broadening, and the solid-state (dispersional and vibrational) broadening as described by de Groot *et al.*,[2] which is currently too complicated to estimate nonempirically. Therefore, in the present paper, the curves obtained by the simple Gaussian broadening are shown together for easy comparison with the experimental spectra.[16]

The SP calculation of the Ti $L_{2,3}$-edge XANES in $SrTiO_3$ reproduced the absolute transition energies of peaks *c*, *d*, *e*, and *f* quite well. In contrast to this, the intensity ratios follow the statistical values $L_3/L_2=2/1$ and $t_{2g}/e_g\sim 3/2$, which are qualitatively opposite to the observed spectrum.

The relative intensities of peaks are drastically improved by the relativistic CI calculation, where the ligand-field multiplet effects considerably decrease both L_3/L_2 and t_{2g}/e_g ratios. Moreover, the small leading peaks *a* and *b* are also reproduced and the resultant theoretical spectrum is in excellent accordance with the observed one. These results are essentially consistent with the atomic multiplet calculation.[13] In order to analyze the origin of each peak in detail, a configuration analysis of the many-electron wave functions has been carried out. Thanks to the orthonormality of the Slater determinants, the composition of the *i*th Slater determinant within the *p*th eigenstate is simply given by $|C_{ip}|^2$. The contributions from each configuration in Table I are shown in Fig. 2, which clearly indicates that peaks *c*, *d*, *e*, and *f* mainly correspond to $(2p_{1/2})^2(2p_{3/2})^3(t_{2g})^1(e_g)^0$, $(2p_{1/2})^2(2p_{3/2})^3(t_{2g})^0(e_g)^1$, $(2p_{1/2})^1(2p_{3/2})^4(t_{2g})^1(e_g)^0$, and $(2p_{1/2})^1(2p_{3/2})^4(t_{2g})^0(e_g)^1$, respectively, and that the small leading peaks *a* and *b* originate from the multiplet splitting of the same configuration with peak *c*.

The SP calculation of the Ni $L_{2,3}$-edge XANES of NiO shows only two peaks corresponding to the transitions to the e_g state, as expected from the complete occupancy of the t_{2g} orbitals in the ground state. Although the absolute transition energies are reproduced quite well, observed fine structures in each edge are missing.

The relativistic CI calculation shows that the ligand-field multiplet effects split each peak and clearly reproduce the fine structures in the experimental spectrum. The configuration analysis attributes peaks *a* and *b* to $(2p_{1/2})^2(2p_{3/2})^3(t_{2g})^6(e_g)^3$ and peaks *f* and *g* to $(2p_{1/2})^1(2p_{3/2})^4(t_{2g})^6(e_g)^3$. Although the small peak *c* mainly corresponds to a two-electron excitation state $(2p_{1/2})^2(2p_{3/2})^3(t_{2g})^5(e_g)^4$, the configuration interaction slightly allows a transition to this state through the small composition of $(2p_{1/2})^2(2p_{3/2})^3(t_{2g})^6(e_g)^3$ in this state.

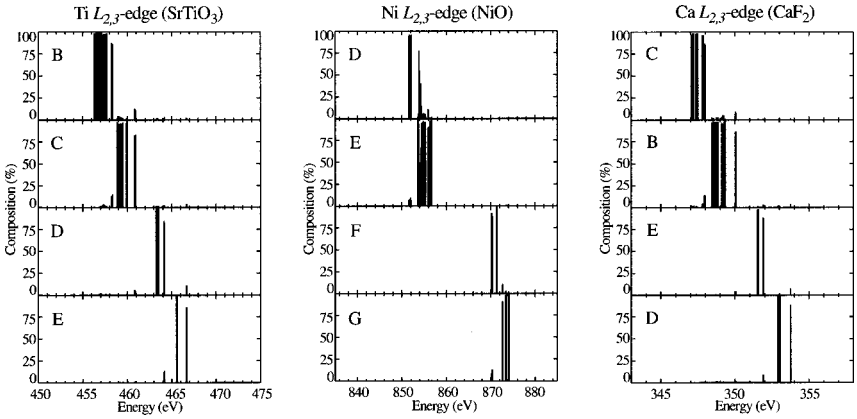

FIG. 2. Configuration analysis of many-electron wave functions corresponding to the final states of the cation $L_{2,3}$-edge XANES using $(TiO_6)^{8-}$, $(NiO_6)^{10-}$, and $(CaF_8)^{6-}$ clusters. The labels represent the electronic configurations listed in Tables I and II.

Similarly, the small shoulder *h* originates from a two-electron excitation state $(2p_{1/2})^1(2p_{3/2})^4(t_{2g})^5(e_g)^4$ interacting with $(2p_{1/2})^1(2p_{3/2})^4(t_{2g})^6(e_g)^3$. In the present calculation, peaks *d* and *e* could not be reproduced because they are attributed to the states relevant to a ligand hole.[17] The present approach can be also easily extended to include the ligand holes by taking into account the molecular orbitals mainly consisting of the ligand orbitals.

The experimental Ca $L_{2,3}$-edge XANES of CaF_2 is at first sight somewhat similar to the Ti $L_{2,3}$-edge XANES of $SrTiO_3$. However, this resemblance is accidental and the origins of the peaks are quite different. The most essential difference is the opposite sign of the octahedral crystal field due to the different coordination number; the former is in eightfold (simple cubic) coordination and the latter is in sixfold (octahedral) coordination. The theoretical spectra by the SP calculation clearly manifest this difference.

Interestingly, this underlying difference is obscured by the totally opposite intensity redistribution between t_{2g} and e_g due to the ligand-field multiplet effects, where the ratio t_{2g}/e_g is increased in the Ca $L_{2,3}$ edge of CaF_2, while it is decreased in the Ti $L_{2,3}$ edge of $SrTiO_3$. The theoretical spectrum of the former based on the relativistic CI reproduces all peaks except a small peak *f*. The origin of this peak is not clear yet, which could not be reproduced in the atomic calculation either.[3] The configuration analysis attributes peaks *b*, *d*, *e*, and *g* to $(2p_{1/2})^2(2p_{3/2})^3(t_{2g})^0(e_g)^1$, $(2p_{1/2})^2(2p_{3/2})^3(t_{2g})^1(e_g)^0$, $(2p_{1/2})^1(2p_{3/2})^4(t_{2g})^0(e_g)^1$, and $(2p_{1/2})^1(2p_{3/2})^4(t_{2g})^1(e_g)^0$, respectively, and the small peaks *a* and *c* to the same configurations with peaks *b* and *d*, respectively.

IV. CONCLUSION

In the present paper, we have demonstrated an excellent predictive power of the relativistic cluster calculation including CI for the reproduction of 3*d* transition-metal $L_{2,3}$-edge XANES and ELNES by showing the results of three simple but contrasting materials ($SrTiO_3$, NiO, and CaF_2). The effect of crystal-field splitting and the effect of hybridization of anion orbitals are included naturally by the use of molecular orbitals. Not only the absolute peak energies, but also their relative intensities are reproduced excellently without any empirical parameters. Such a nonempirical approach can directly correlate the observed spectra with the actual local atomic arrangements and hence is indispensable for the full utilization and proper interpretation of the recent accumulation of experimental XANES and ELNES for a variety of advanced materials.

ACKNOWLEDGMENTS

We are grateful to Professor J. Kawai for his valuable discussions. This work was supported by a Grant-in-Aid for Scientific Research from the Ministry of Education, Science, Sports and Culture.

[1] J. Stöhr, *NEXAFS Spectroscopy* (Springer, Berlin, 1992).
[2] F. M. F. de Groot, J. C. Fuggle, B. T. Thole, and G. A. Sawatzky, Phys. Rev. B **41**, 928 (1990).
[3] F. M. F. de Groot, J. Electron Spectrosc. Relat. Phenom. **67**, 529 (1994).
[4] J. van Elp, H. Eskes, P. Kuiper, and G. A. Sawatzky, Phys. Rev. B **45**, 1612 (1992).
[5] S. Watanabe and H. Kamimura, Mater. Sci. Eng., B **3**, 313 (1989).
[6] J. C. Slater, *Quantum Theory of Molecules and Solids* (McGraw-Hill, New York, 1974), Vol. 4.
[7] A. Rosén, D. E. Ellis, H. Adachi, and F. W. Averill, J. Chem. Phys. **65**, 3629 (1976).
[8] J. Onoe, H. Nakamatsu, T. Mukoyama, R. Sekine, H. Adachi, and K. Takeuchi, Inorg. Chem. **36**, 1934 (1997).
[9] K. Ogasawara, T. Ishii, I. Tanaka, and H. Adachi, Phys. Rev. B **61**, 143 (2000).
[10] H. Kanda, M. Yoshiya, F. Oba, K. Ogasawara, H. Adachi, and I. Tanaka, Phys. Rev. B **58**, 9693 (1998).
[11] I. Tanaka, H. Araki, M. Yoshiya, T. Mizoguchi, K. Ogasawara, and H. Adachi, Phys. Rev. B **60**, 4944 (1999).
[12] T. Mizoguchi, I. Tanaka, M. Yoshiya, F. Oba, K. Ogasawara, and H. Adachi, Phys. Rev. B **61**, 2180 (2000).
[13] F. M. F. de Groot, Z. W. Hu, M. F. Lopez, G. Kaindl, F. Guillot, and M. Tronc, J. Chem. Phys. **101**, 6570 (1994).
[14] G. van der Laan, Phys. Rev. B **41**, 12 366 (1990).
[15] L. A. Montoro, M. Abbate, E. C. Almeida, and J. M. Rosolen, Chem. Phys. Lett. **309**, 14 (1999).
[16] The adopted values of the full width at half maximum is 1.0 eV for Ti and Ni and 0.4 eV for Ca.
[17] G. van der Laan, J. Zaanen, G. A. Sawatzky, R. Karnatak, and J.-M. Esteva, Phys. Rev. B **33**, 4253 (1986).